

BARNET: Towards Activity Recognition Using Passive Backscattering Tag-to-Tag Network

Jihoon Ryoo⁺, Yasha Karimi, Akshay Athalye, Milutin Stanačević,
Samir R. Das, Petar Djurić
Stony Brook University, ⁺SUNY Korea

ABSTRACT

We present the vision of BARNET (Backscattering Activity Recognition Network of Tags), a network of passive RF tags that use RF backscatter for tag-to-tag communication. BARNET not only provides identification of tagged objects but also can serve as a ‘device-free’ activity recognition system. BARNET’s key innovation is the concept of backscatter channel state information (BCSI) which can be measured via systematic multiphase probing of the backscatter tag-to-tag channel using innovative processing on the passive tags. So far such measurements were only possible using active radio receivers that consume much higher power. Changes in BCSI provide signatures for different activities in the environment that can be learned using suitable machine learning tools. We develop the BARNET tag architecture which shows that an ASIC implementation can run on harvested RF power. We develop a printed circuit board (PCB) prototype using discrete components to evaluate activity recognition performance. We show that the prototype can recognize human daily activities with an average error around 6%. Overall, BARNET uses passive tags to achieve the same level of performance as systems that use powered, active radios.

CCS CONCEPTS

- **Computer systems organization** → **Sensor networks** ;
- **Hardware** → *Networking hardware; Wireless devices*;

1 INTRODUCTION

We imagine a future where our physical environment is cyber-enabled in its finest detail. Most, if not all, physical objects are tagged for identification and tracking. Moreover, the tags are also able to sense activities and interactions around them. This provides a form of ambient intelligence. This work develops a foundational technique to enable this vision by marrying two enabling technologies:

- Battery-less RF-powered tags with direct tag-to-tag communication ability [28, 33, 39]. They are like RFID tags [17, 18] but differ in one critical aspect – they can

communicate among themselves without the need for active¹ radio-based device such as an RFID reader.

- ‘Device-free’ activity recognition (e.g., [50]) for inferring activities via analysis of RF signals reflected from objects and living beings in the surrounding environment.²

The marriage of these two disparate technologies empowers an autonomous network of RF-powered tags with the ability to recognize activities in the surrounding environments via a form of RF sensing without any active radio device. The unique contribution of this work is to develop a foundational technique to enable RF-powered battery-less tags equipped only with passive receivers to perform wireless channel estimation using near zero-power techniques. The tags are also able to perform multihop tag-to-tag communication [42] and thus can form autonomous intelligent networks without direct help from high-powered components such as access points or RFID readers. We call the proposed design BARNET (‘B’ackscattering ‘A’alytics and Activity ‘R’ecognition ‘N’e’twork of ‘T’ags). To achieve its goals, BARNET tags use i) novel communication techniques for channel measurement based only on passive backscattering of external RF signals and ii) exploit these measurements to perform analytics and to discover and interpret meaningful patterns in the collected data. BARNET derives its power from significant redundancy where all physical objects are RF tagged and thus a large number of tags are always available in the neighborhood.

To understand potential impact of BARNET, see Figures 1(a) and (b). The first sub-figure (a) describes the scenario where the channel between RF tags and an active radio transceiver (e.g., RFID reader) is monitored. The sub-figure (b) depicts BARNET wherein tags are capable of monitoring channels between one another. This automatically can exploit $O(n^2)$ channels as opposed to only $O(n)$ channels. Additionally, BARNET does not require communication with active radio devices for its operation and is, in principle, able to use any appropriate external RF signal, whether ambient or intentionally generated, as carrier for the backscatter communication (Figure 1(b)). This ability to build autonomous networks without the need for a central active radio communication controller automatically enhances the scalability of BARNET as compared to conventional active reader based systems (Figure 1(a)).

Permission to make digital or hard copies of all or part of this work for personal or classroom use is granted without fee provided that copies are not made or distributed for profit or commercial advantage and that copies bear this notice and the full citation on the first page. Copyrights for components of this work owned by others than ACM must be honored. Abstracting with credit is permitted. To copy otherwise, or republish, to post on servers or to redistribute to lists, requires prior specific permission and/or a fee. Request permissions from permissions@acm.org.

MobiSys '18, Munich, Germany

© 2018 ACM. ISBN 978-1-4503-5720-3/18/06...\$15.00

DOI: <https://doi.org/10.1145/3210240.3210336>

¹We use the terms ‘active’ vs ‘passive’ to indicate devices that require on-board power source as opposed to being powered by externally generated RF signals.

²The term ‘device-free’ signifies that the techniques do not require these objects or beings carry any tag or device.

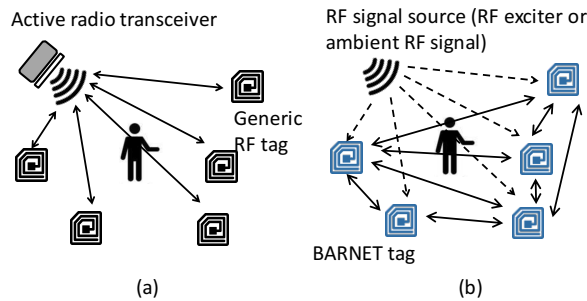


Figure 1: (a) Traditional RFID system, (b) Proposed BARNET system. Unlike traditional RFID, BARNET is capable of tag-to-tag backscatter communications as well as activity sensing on the tag-to-tag channel. This enables scalable deployment (no active radio) as well as sensing on many more channels ($O(n^2)$).

1.1 Passive RF Sensing of Backscatter Channel

BARNET is a network of passive batteryless tags with a limited computational ability that i) directly communicate among themselves via *backscatter modulation* of an external RF signal and ii) can measure and record variations in the backscatter wireless links. The tags are attached to everyday objects identifying them, much like in RFID systems except that conventional RFID reader devices are not needed. Tags could also be part of the building infrastructure such as wall or ceiling panels. RF exciters supply RF power and provide the signal used for backscattering, but otherwise have no intelligence. If strong enough ambient RF signals are available (e.g., TV signals or WiFi [10, 28, 33]) they can proxy for exciters. See Figure 1(b). Thus, intentionally deployed exciters are not critical for the fundamental techniques described here.³ Some of tags (sink nodes) are attached to embedded platforms that in turn connected via IP networks to an analytics server that executes necessary machine learning functions. These embedded platforms are basically gateways between the tag network and external world - they do not need any RF communication ability.

The multipath wireless channel between two passive tags undergoes changes related to dynamic alterations in their vicinity. BARNET exploits a fundamental characteristic of this tag-to-tag backscatter link: amplitude of the received backscatter at an Rx tag varies based upon the phase of the channel between the two tags. Then, by systematically varying the phase of the Tx signal and quantifying the Rx signal amplitude for various Tx phase values, we are able to formulate a channel estimation technique for the radio-less tags. *Such measurement capability previously was limited to devices capable of IQ*

³However, it is important to note that while recent literature [10, 28, 33] has promoted use of ambient signals for backscatter communication, the actual power levels used in these papers are unusually high relative to what could normally be typically expected in ambient settings [40].

demodulation that requires significantly higher power. This innovation is central to the passive tags that form the building blocks in BARNET. Together with the communication and measurement protocols, innovative hardware design and sensor fusion BARNET forms a truly ubiquitous and scalable passive tag network that can simultaneously provide identification and activity recognition ability.

1.2 Contributions

In this paper we describe the BARNET vision and develop the foundational principles underlying wireless channel measurements using passive techniques that is central to BARNET. We develop and analyze the basic tag design and show experimental results that demonstrate: (i) the feasibility of the proposed passive channel measurement techniques, and (ii) the usefulness of such channel measurements in recognizing human activities in the surrounding space. The tag design and power analysis are based on ASIC implementation to ensure very low power operation using harvested RF power. However, the experimental demonstration uses discrete off-the-shelf components integrated on a printed circuit board (PCB) that closely approximates the ASIC design, but has a higher power consumption.

The specific contributions are summarized as follows:

- **Passive techniques for backscatter channel measurements (Section 3):** We develop the concept of backscatter channel state information (BCSI). We show via analysis how BCSI can be measured by systematic multiphase probing of the backscatter channel. We develop the necessary protocol support for multiphase probing and recording the BCSI features.
- **RF-powered tag architecture (Section 4):** We develop a tag design capable of i) tag-to-tag backscatter communication and ii) BCSI measurements based on the above concept. We perform a power analysis showing that the tag is able to operate using harvested RF power when implemented as an ASIC.
- **Experimental demonstration (Section 5)** We use tag prototypes to experimentally demonstrate the BCSI's ability to characterize the backscatter channel and recognize daily human activities.

2 BACKGROUND AND CHALLENGES

BARNET draws on two sets of fundamental advances in recent years. We describe these advances below to outline a context and describe the challenges.

2.1 Device Free Activity Recognition using Wireless Signals

The human body is a reflector of RF signals and hence human activities can be recognized by analyzing dynamic variations of certain parameters of reflected signals. This enables activity recognition without the need for humans to carry any sensors or devices (i.e. 'device-free'). Almost all of the related research efforts employ some kind of 'active' wireless communication link for this purpose. Such links have powered radio

transceivers. (WiFi has been often used due to its popularity.) In such a link, the signal at the receiver S_R at any time t can be expressed as $S_R(t) = A_R e^{j(\omega t + \theta)}$, where A_R and θ are the amplitude and phase respectively of the received signal at time t , and $\omega = 2\pi f$, where f is the carrier frequency. Human activities produce dynamically varying reflections that affect A_R and θ . The active receivers possess on-board radios with a *local oscillator* operating at the carrier frequency. This enables the well-known I-Q demodulation [22] providing the receiver with a straightforward mechanism to measure both A_R and θ . Wireless device-free systems are based on observing dynamic variations in these or related channel parameters and extracting patterns correlating to known activities. The activity signatures are inferred from dynamic variations in the channel in response to the activity rather than from static signal levels. As a result, such systems are agnostic to their deployment environment [50].

Based on the basic principle above, prior research has described activity recognition systems using a variety of active transceivers (e.g. USRP radio) and analysis approaches [8, 9, 24, 41, 45, 49]. A particularly appealing commodity-based approach uses existing WiFi chipsets to extract so-called *Channel State Information (CSI)* [19, 30, 51, 55]. CSI describes amplitude and phase of each OFDM subcarrier between each Tx-Rx antenna pair and provides the added benefit of frequency and antenna diversity [21, 52]. A central theme in these approaches, however, is the dependence on high power active radio receivers for complex signal processing. This limits scalability and the spatial granularity of measurements because the number of such receivers per unit deployment area is small.

2.2 Backscattering Tag-to-Tag Communication

In BARNET we are specifically interested in passive, battery-less RF-powered tags to perform similar activity recognition. The idea of passive RF tags has been the most widely employed in RFID (Radio Frequency IDentification) technology [11, 13, 16–18, 20, 47, 48]. However, such RFID tags can only communicate with a high power active radio, viz. the RFID reader. Activity recognition systems indeed have been built using RFID [25, 32, 38] but using processing on the reader-side only (Figure 1(a)). BARNET removes this limitation by making such processing possible directly on the tag (Figure 1(b)). To understand the challenges of such on-tag processing, let us first describe the regular RFID tag-reader link.

2.2.1 RFID Technology: Tag-Reader Link. In an RFID system, the reader provides a continuous wave (CW) RF signal, contains an active radio and has a relatively powerful embedded processor. Almost the entire intelligence and complexity in the RFID system is on the side of the reader. The tag is entirely powered by the signal from the reader. The modulated signal from the reader to the tag (Figure 2) typically has a very high *modulation index*.⁴ The modulated RF signal emitted by the reader is demodulated using a ‘passive’ envelope

⁴Modulation index is the ratio of the difference and average of the amplitudes of the input RF signal for logic ‘1’ and ‘0’.

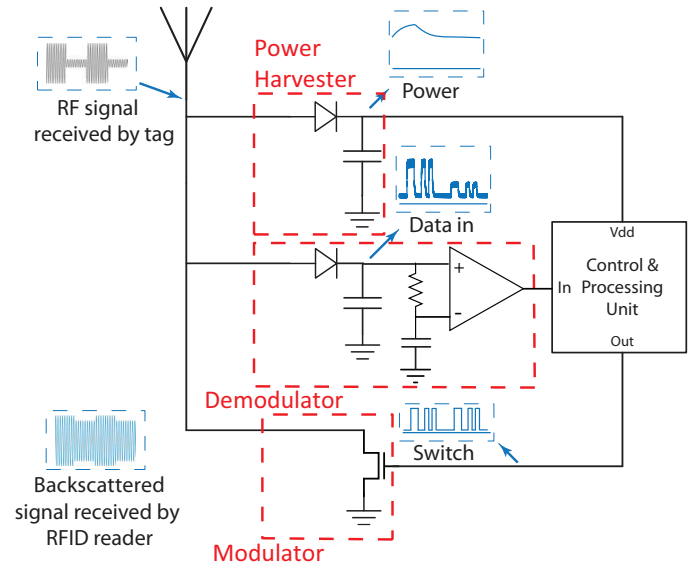


Figure 2: RFID tag architecture showing various signals

detector circuit. Due to the high modulation index, the bits are easily resolved by a comparator that follows the envelope detection [17, 18], as illustrated in Figure 2. The comparator is the only component that needs power other than the control and processing units. The tag still works in near-zero power regime with only the harvested RF power as power source.

For tag-to-reader communication, the tag simply modulates its antenna reflection coefficient by switching between two impedances that terminate the tag antenna circuit [17, 18] and reflects back the reader signal. This is the well-known *backscattering* communications principle [12]. The *backscatter signal received at the reader, however, has a low modulation index*, as the reflected RF power from the tag is small when it reaches the reader traveling twice the distance between the reader and the tag. The reader can indeed demodulate this signal, but unlike the tag it employs IQ demodulation and active cancellation of the interfering carrier signal. This processing is key to the reader’s ability to decode the tag signal error-free.

While such conventional RFID technology has been employed for activity recognition using reader side processing, the only work in our knowledge that attempts to do this on passive RF tags is [29] where such tags are connected to smart phones. The BARNET approach eliminates the need for high power radios completely either for communication or for activity sensing. This eliminates the need for readers, access points or similar devices, thus improving scalability for ubiquitous deployment.

2.2.2 Backscattering Tag-to-Tag Link. Recent work [27, 33, 35, 37, 39, 44] has demonstrated that passive tags can communicate among themselves without any reader. In this case, the RF signal for backscattering can come from RF exciters that provide CW signals but otherwise do not have any intelligence.

Use of ambient RF signals is possible if they have enough power to provide the needed excitation [33]. Our goal is to impart the tag-to-tag link an ability to measure and characterize the backscatter wireless channel for recognizing activities in the surrounding areas.

Before describing specific challenges, let us first describe the signal level operation of the tag-to-tag backscatter link. See Figure 3. The Tx tag backscatters the external excitation signal, but now the signal must be demodulated by a passive Rx tag. The signal observed at the Rx tag is superposition of the excitation signal and the backscatter signal from the Tx tag (plus corresponding signal reflections from the environment). Assume that the Tx tag is modulating the backscatter by changing the input impedance between two states. In the first state, antenna circuit is open and the signal backscattered by the Tx tag can be neglected. The received signal in this state can be written as:

$$v_{R1}(t) = A_E(t)e^{j(\omega t + \theta_E(t))} \quad (1)$$

where A_E is the amplitude and θ_E is the phase of the signal received at Rx tag. These parameters, A_E and θ_E , define the *exciter-Rx* channel. In the second state Tx tag reflects the incident RF signal with a change in the phase ϕ . The received signal at the Rx tag which is a superposition of the exciter signal and the backscatter signal can be written as:

$$v_{R2}(t) = A_E(t)e^{j(\omega t + \theta_E(t))} + A_B(t)e^{j(\omega t + \theta_B(t) + \phi)} \quad (2)$$

A_B is the amplitude of the backscatter and θ_B is the phase of the *exciter-Tx-Rx* channel in the received signal. In the case of an activity in the surrounding of the tags, Figure 3 illustrates the change in the reflection paths that contribute to both v_{R1} and v_{R2} signals. The passive envelope detector only provides the amplitude of the received signal. When the amplitude of the backscatter signal A_B is much smaller than the amplitude of the excitation signal A_E (i.e., $A_B/A_E \ll 1$), which is almost always the case in BARNET, the difference in the amplitudes of the received signals in two states becomes⁵:

$$\Delta v_R(t) = v_{R2}^{amp}(t) - v_{R1}^{amp}(t) = A_B \cos(\phi + \theta_B(t) - \theta_E(t)) \quad (3)$$

The difference between the amplitude in two states, Δv_R , is the signal that demodulator of the Rx tag has to resolve after the envelope detection. We denote the phase difference between the *exciter-Rx* and *exciter-Tx-Rx* wireless channels as $\theta_{BC}(t) = \theta_B(t) - \theta_E(t)$, and call it *backscatter channel phase*.

The major challenge in the design of backscattering tag-to-tag link is that now the tag has to resolve a low modulation index signal that it receives from the Tx tag. Modulation index in the signal after envelope detector, with the same approximation ($A_B/A_E \ll 1$), is $\Delta v_R/A_E$. Additionally, the difference in the amplitudes Δv_R in the modulated signal depends not only on the amplitude of the backscatter A_B , but also on the phase difference between signals received at Rx tag from the exciter and from Tx tag. This means that Δv_R can go down to zero depending upon the instantaneous phase θ_{BC} making it harder for the demodulator. This can be

⁵This is derived from (1) and (2) by observing that $|\frac{A_B}{A_E}| \ll 1$ and then applying the Binomial approximation, $(1+x)^n \approx (1+nx)$

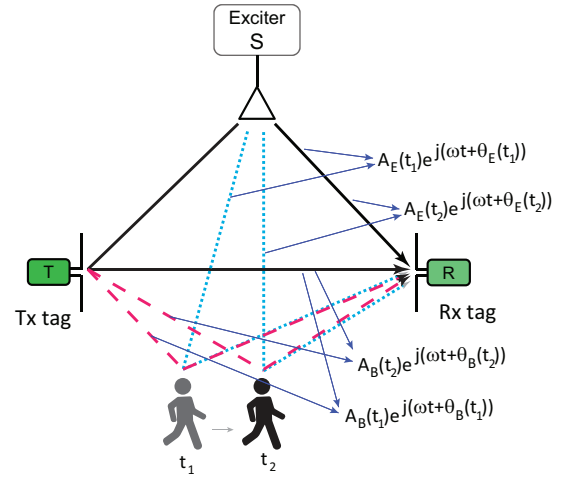


Figure 3: The direct path and reflection signals in backscattering tag-to-tag link scenario at two different time instants.

addressed by changing the phase ϕ on the Tx tag [44]. This is the approach we follow, but do not further elaborate in this paper as we will solely focus on the activity recognition aspects.

3 FOUNDATIONAL TECHNIQUES OF BARNET

The backscattering tag-to-tag link comprises two wireless channels, *exciter-Rx* and *exciter-Tx-Rx*, that are affected by the activity in the surroundings. The goal of BARNET is to enable measurement of the dynamics of these channels and use it for activity recognition. If we are able to estimate amplitudes and phases of these two channels, or a significant subset of them, the properties and performance of this activity recognition technique would be similar to the conventional RF activity recognition techniques outlined in Section 2.1, but with the greatly added benefits of increased spatial granularity and link diversity as stated in Section 1. However, as we have elaborated in the previous section, the passive Rx tag has an envelope detector that can only detect the the amplitude difference $\Delta v_R(t)$ in resultant backscatter signal given by equation (3). Without the ability to perform IQ demodulation like in an active wireless receiver (Section 2.1), the passive Rx tag does not have any inherent ability to determine the backscatter amplitude A_B or the backscatter channel phase θ_{BC} . Hence a generic passive tag cannot perform the dynamic channel estimation needed for activity recognition. A central innovation in BARNET is a novel communication technique that overcomes this limitation and imparts passive tags the ability to estimate the channel in real time by determining both A_B and θ_{BC} without the need for active IQ demodulation. This technique is based on *multiphase probing* (MPP) of the backscatter channel between a pair of tags, wherein the Tx tag sends out the systematically designed MPP signal (see

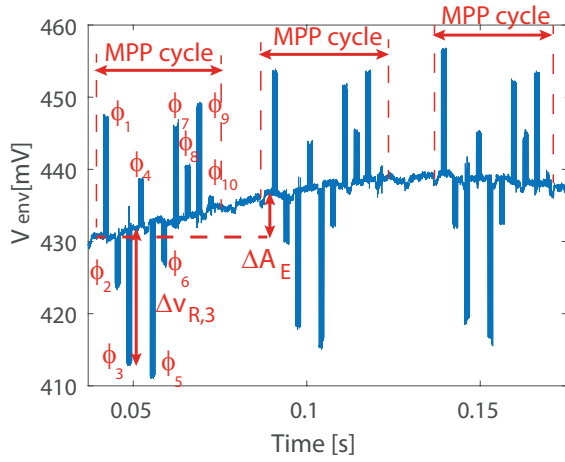


Figure 4: The received signal after envelope detection with denoted measured signals

below) which in turn enables the Rx tag to estimate channel parameters.

Empowered with this ability for channel estimation using passive tags, BARNET can (1) measure wireless channel dynamics at multiple tags in a distributed manner and (2) ‘fuse’ these distributed measures centrally for improved estimation. As highlighted in Section 1, this concept amounts to a paradigm shift by enabling use of passive tag networks for activity recognition and physical analytics, applications which have, so far, been almost exclusively restricted to the realm of active radio systems.

3.1 Multi-Phase Probing (MPP) of Backscatter Channel

To demonstrate our proposed technique, we once again consider a single passive tag-to-tag link shown in Figure 3. As derived in Equation 3, when the Tx tag backscatters, the amplitude difference (for the two antenna states) detected at the Rx tag using passive envelope detection is $\Delta v_R = A_B \cos(\phi + \theta_{BC})$ where A_B is the backscatter amplitude, θ_{BC} is the backscatter channel phase, and ϕ is the phase introduced by the Tx backscatter modulator. A key observation here is that the parameters A_B and θ_{BC} vary randomly based on the dynamics of the environment. However, ϕ is deterministic and fixed by the Tx modulator and remains unaffected by environmental dynamics. We use this key property in developing our MPP technique for backscatter channel estimation.

Now, we consider a Tx tag with a modulator that can backscatter with K different unique phases $\phi_1, \phi_2, \dots, \phi_K$. We refer this modulator as capable of backscattering in K phase slots with each slot characterized by its Tx phase ϕ_k . The MPP signal consists of a short bit sequence backscattered successively over all available K phase slots. Then the signal detected by

the Rx tag in each slot becomes:

$$\Delta v_{R,k} = A_B \cos(\phi_k + \theta_{BC}), k = 1, 2, \dots, K \quad (4)$$

Figure 4 illustrates the envelope detected received signal for 3 successive transmissions (or 3 phase slots) of the MPP signal. The Rx tag measures $\Delta v_{R,k}$ for each slot while the characteristic phase ϕ_k of each slot are known and fixed by the hardware. Then, from Equation 4 the Rx tag can determine the key channel parameters A_B and θ_{BC} as

$$\theta_{BC} = \frac{\pi}{2} - \phi_k \Big|_{\Delta v_{R,k}=0} \quad \text{and} \quad A_B = \Delta v_{R,k} \Big|_{\phi_k = -\theta_{BC}} \quad (5)$$

Accordingly, the Rx tag can estimate θ_{BC} based on which value of ϕ_k results in $\Delta v_{R,k} = 0$. It does this 1) by detecting the two phase slots between which zero-crossing of Δv_R occurs and 2) then doing a weighted interpolation between these phases. After having estimated θ_{BC} , the Rx tag knows the exact phase slots between which the latter condition in Equation 5 will be satisfied. It then estimates A_B by weighted interpolation of $\Delta v_{R,k}$ between these phases. The coefficients of this interpolation is the same as those used in estimation of θ_{BC} . In this way, using the MPP technique, BARNET can estimate the channel parameters A_B and θ_{BC} based only on the reception of Δv_R without the need for any active demodulation. We will describe the BARNET tag architecture for implementing this technique in Section 4.

3.2 Backscatter Channel State Information (BCSI)

As described in Section 2.2.2, in backscattering tag-to-tag link, we are monitoring activity through two wireless channels; viz. the *exciter-Rx* channel characterized by amplitude A_E and phase θ_E and the *exciter-Tx-Rx* channel characterized by A_B and θ_B . In the previous subsection, we have demonstrated that using the MPP technique the Rx tag can measure the parameters, amplitude A_B and phase $\theta_{BC} := (\theta_B - \theta_E)$. In the *exciter-Rx* channel, in the absence of backscatter signal, we can passively measure only amplitude of v_{R1} by monitoring the output of the envelope detector (Equation 1). Since we cannot control the exciter behavior, we cannot measure the dynamics of this *exciter-Rx* channel using an MPP like mechanism. However, by recording the changes in the excitation level A_E between successive MPP cycles, we can extract valuable supplementary information about this channel to aid in activity recognition. We refer to this recorded value as ΔA_E and it is illustrated in Figure 4.

Putting the above techniques together, we formulate a measure for the backscatter channel referred to as the *backscatter channel state information (BCSI)*. This consists of the following three quantities:

- 1) backscatter channel phase θ_{BC} ,
- 2) backscatter amplitude A_B , and
- 3) change in excitation amplitude between two MPP cycles ΔA_E .

This BCSI vector at time t , denoted by

$$\mathbf{h}(t) = [\theta_{BC}(t) \quad A_B(t) \quad \Delta A_E(t)],$$

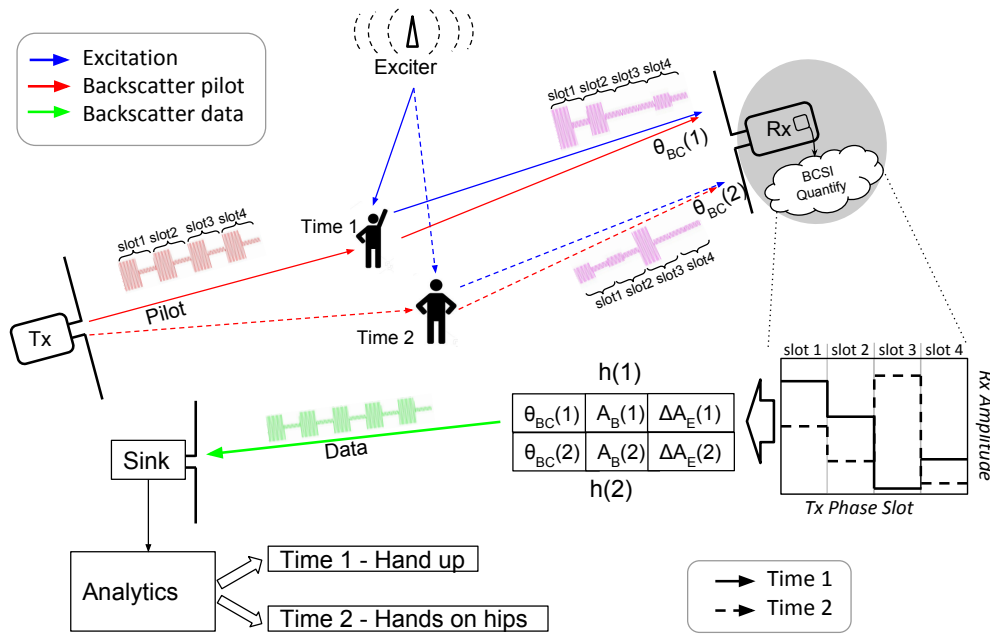


Figure 5: BARNET network showing two tags and one sink node.

is then used as as feature vector which forms the basis of activity recognition in BARNET.

3.3 BARNET Operation

To demonstrate how BARNET functions, we consider a situation with some human activity (movements) happening in the vicinity of a tag-to-tag link as shown in Figure 5. We first assume that there is only a pair of tags present in the vicinity of the activity. We will later describe how a larger number of tags would sense and process information. When there is no activity in the vicinity of the tags, they largely remain idle and just sense the excitation signal amplitude A_E for changes in the environment. When a change in excitation signal is detected, tags start channel estimation whereby one tag becomes the Tx tag and starts sending out the MPP signal. We depict two time instances during a specific movement being performed, thus altering the backscatter channel between the two tags. We denote the resultant backscatter channel phase of the two instances as $\theta_{BC}(1)$ and $\theta_{BC}(2)$ (solid lines for instant 1 and dotted line for instant 2). At both instances, the Tx tag sends out the MPP over four different phase slots.

Figure 6 shows the format of the MPP signal packet. The packet begins with self-identifier indicating which Tx tag the MPP originates from. This is followed by a short synchronization random number (SRN) which is used for time synchronization when analyzing BCSI vectors sent from one Tx tag received simultaneously at multiple Rx tags. Finally, the packet includes the multiphase probe consisting of short slot identifiers sent over the respective phase slots with brief delimiters separating them. This forms one cycle of MPP at time

t . The Rx tag processes this signal and estimates the aforementioned BCSI vector. The Rx tag records the Tx identifier, the synchronization random number (SRN), and then serially records the BCSI feature vector, consisting of the values $\theta_{BC}(t)$, $A_B(t)$ and $\Delta A_E(t)$. The process of MPP transmission and BCSI vector recording is then repeated throughout the duration of activity, each time incrementing the SRN in Tx packet by 1. The sampling time of the BCSI vector estimation is product of the backscattering time at a single phase ϕ_k and the number of phase slots K . The sampling rate is sufficiently higher than the frequency/speed of the activities. The determination of the sampling rate is also driven by the energy budget of the Rx tag that limits the backscatter data rate and the number of phase slots.

Our proposed technique is agnostic to deployment environment. This is because it utilizes phase diversity by introducing a fixed, deterministic phase offset in each Tx phase slot. As a result, the instantaneous phase difference between the received signals in successive slots (i.e. within a single MPP packet) is always fixed, irrespective of the environmental clutter. Due to the location invariance, the sampled BCSI vector collected for a specific activity in an environment will have similar signature to the same activity performed in a different environment, as well as activity performed by a different person. This also means that the training of a classification algorithm based on the recorded BCSI information can be performed in a specific environment for a set of selected activities and the obtained support vectors can be used for classification in a different environment.

The classification task can be performed at different levels of BARNET. The support vectors can be stored locally on each

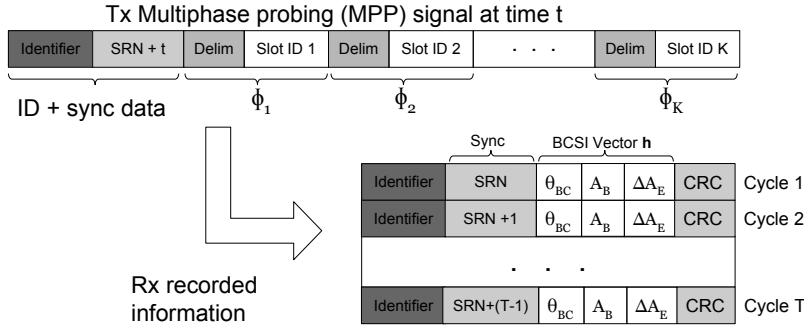


Figure 6: Transmission and reception of MPP signal

Rx tag and the classification task can be performed on tag if the energy budget permits. The BCSI measurement, along with the identifier of the Rx tag, can also be conveyed to a sink node using multihop relaying for computation, as illustrated in Figure 5.

In the case of multiple tags in the vicinity of the activity, a single tag will act as the Tx tag at a time, sending out MPPs and other neighboring tags will serve as Rx tags recording BCSI information. Aloha-based collision arbitration will be used in the MAC layer for giving the channel to a single Tx tag. As shown in Figure 6, the “Identifier” and “Sync” fields in the recorded Rx information will indicate simultaneous BCSI measures for multiple Rx tags from the same Tx tag. Hence these concurrent BCSI measures provide diversity that can exploited centrally to further improve the activity classification accuracy.

4 BARNET RF TAG ARCHITECTURE

In order to operate purely using power harvested from ambient energy or dedicated exciter, the BARNET tag will have to be implemented as an Application Specific Integrated Circuit (ASIC). To demonstrate the feasibility of such a tag with the functionality described in Section 3, we propose a hardware architecture for this tag and then determine its power budget. The circuits for measurement of BCSI are designed and simulated for determination of the power consumption, while the power consumption of conventional building blocks is estimated based on the reported designs in the literature.

4.1 Tag Architecture

The architecture of the BARNET tag in an ASIC implementation is shown in Figure 7(a). A conventional backscattering tag integrates the following modules: RF energy harvester, power management logic and super-capacitor for generation of power supply voltage and storage of extra harvested energy beyond instantaneous consumption; modulator, demodulator and communication control logic to enable backscatter tag-to-tag communication and memory. See, e.g., [27, 33] for examples. To enable on-tag activity recognition, the BARNET tag enhances the backscatter modulator to enable it to send the MPP signal. It also enhances the demodulator/receiver module, shown in Figure 7(b), to make it capable of performing the measurement of voltage signals Δv_R and ΔA_E along with the

computational logic for the BCSI estimation based on the measured voltages. In the description that follows we highlight the design of the enhanced modulator and demodulator.

4.1.1 Multi-Phase Backscatter Modulator. The Tx tag generates the MPP signal by reflecting the incident excitation signal with a different reflection phase. This is achieved by switching the tag antenna impedance between a range of systematically designed impedance values via a multi-port RF switch. Each such impedance corresponds to a phase slot available to the MPP signal. The reflecting phases span the range from $-\pi/2$ to $\pi/2$ uniformly. The number of different phase slots is trade-off between resolution, time required for the MPP transmissions and power consumption.

4.1.2 BCSI Measurement and Demodulation. The mixed-signal front-end of the BCSI estimator converts the voltages $\Delta v_{R,k}$ and ΔA_E to digital values within a single probing cycle, while the estimates of A_B and θ_{BC} are obtained from the digital samples of $\Delta v_{R,k}$ using computational means as explained in Section 3.1. The most stringent constraint in the design of the front-end of the BCSI estimator is power consumption. The simplest approach for obtaining the digital values of $\Delta v_{R,k}$ and ΔA_E would be to apply analog-to-digital converter (ADC) to the output of the envelope detector and then in digital domain find $\Delta v_{R,k}$ and ΔA_E . However, the envelope detector signal depends on the incident power at Rx tag. As the incident power at Rx tag depends on the distance from the exciter, it has a large variation, leading to a wide-range signal at the output of the envelope detector. To convert such signal to digital domain, it would require use of a high-resolution ADC as we are interested in a very small amplitude differences that appear in this signal. The high-resolution ADC would have a prohibitively high power consumption for RF powered tag. This calls for different techniques that will leverage the ultra low-power analog and mixed-signal signal processing to separately obtain $\Delta v_{R,k}$ and ΔA_E first in the analog domain and then use a low-power low-resolution ADC to convert them to digital values.

Measuring ΔA_E . Figure 4 shows the received signal by the Rx tag after envelope detection when the Tx tag sends the MPP. As illustrated in the figure, we are measuring ΔA_E as the difference between amplitudes of the excitation signal A_E at the start of the successive MPP cycles. To reduce the effect of

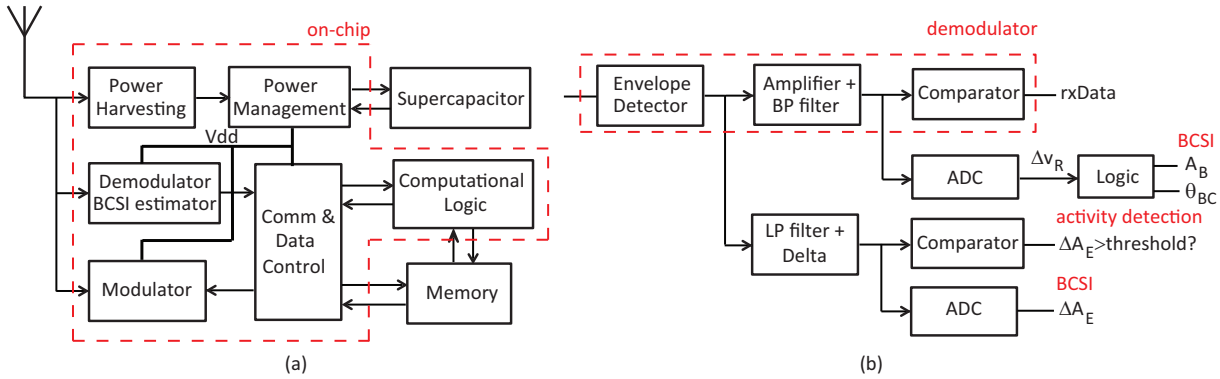


Figure 7: Block diagrams: (a) BARNET tag architecture in an ASIC implementation, (b) demodulator/BCSI estimator block shown in more detail.

the irrelevant small changes in the environment and of noise in the measurement, we apply passive low-pass filter to the excitation signal A_E prior to the subtraction. The excitation amplitude A_E is first sensed in analog domain by sampling the value of the A_E at the start of the MPP cycle and at the start of the subsequent cycle, it is subtracted from the current value of A_E . This analog value that represent ΔA_E , obtained by the sampled difference amplifier, is then be converted to the digital domain using low-resolution, low-power ADC. Successive approximation ADCs are very low power and based on the similar implementations in the literature [23, 43] we can expect a power consumption on the order of 10s of nW at kSamples/s sampling rate.

Measuring $\Delta v_{R,k}$. The envelope detector signal comprises a high pedestal signal corresponding to the excitation signal amplitude A_E (around 430 mV for a specific setup scenario illustrated in Figure 4) and a small variation on top of the large pedestal, signal $\Delta v_{R,k}$ (up to 20 mV in the same illustrated scenario), that has to be measured. To resolve the signal $\Delta v_{R,k}$, we use the same analog front-end architecture as in the demodulator that has been previously reported in [27]. Analog front-end comprises integrated band-pass filtering and amplification. The high-gain amplifier is implemented as the low-noise, low-power folded-cascode amplifier. The high-pass filtering reduces the pedestal value and only the small signal on the top of the pedestal is amplified. The output voltage signal amplifier with integrated high-pass filter, is then converted to the digital domain using a similar architecture of ADC, as the one used in the measurement of ΔA_E .

Demodulation. The amplifier with integrated band-pass filter used for measurement of $\Delta v_{R,k}$ is shared by the demodulator to demodulate data bits. The small amplitude baseband signal is easily resolved with implementation of a low-power comparator [27].

4.1.3 Activity Detector. The detection is implemented through comparison of the excitation amplitude A_E and time-delayed version of the same signal, with the comparator as the only active component. The power consumption of the activity detector must be minimized as this circuit will be operating

continuously as long as tag is active even if there is no activity in the environment. Also, the detector must operate while the tag is harvesting RF energy. This means that the detector design has to be co-optimized with the design of the power harvesting circuit. These are more circuit-level explorations and we plan to pursue these in future work.

4.2 Analysis of Power Consumption

To demonstrate the feasibility of BARNET tag operating on RF harvested power, we estimate the power consumption of proposed tag architecture. The power consumption of the proposed architecture of the modulator and demodulator with BCSI estimator is obtained through the simulations. We have designed and simulated the demodulator/BCSI estimator in 45 nm CMOS technology. Keysight Technology’s Advanced Design System (ADS) and Cadence Virtuoso are used for the design and simulation. The detailed circuit implementation of demodulator, comprising the analog front-end (amplifier and band-pass filter) and the comparator has been reported in [27]. Along with the the analog front-end for measurement of ΔA_E that comprises passive low-pass filter and sampled difference amplifier, the demodulator/BCSI estimator without two ADCs consumes $1.4 \mu W$. The ADCs for BCSI estimation can be implemented using the successive approximation ADC architecture. Based on the similar implementations in the literature [23, 43], we estimate a power consumption of each ADC to be in the order of 100 nW at kSamples/sec sampling rate, leading to the overall estimated power budget of $1.6 \mu W$ for the demodulator/BCSI estimator. The multi-phase backscatter modulator, which is essentially an RF switch, consume a fraction of the power of the demodulator/BCSI estimator.

The additional building blocks include computational logic and memory. The computation is needed for BCSI vector estimation, implementation of the algorithms for tag operation control and classification with stored support vectors. Based on the implementation of processors with similar computational logic and memory capacity in the literature [15, 26, 34, 36], we can estimate that the power consumption of these blocks is on order of few μW s. It is important to note that while

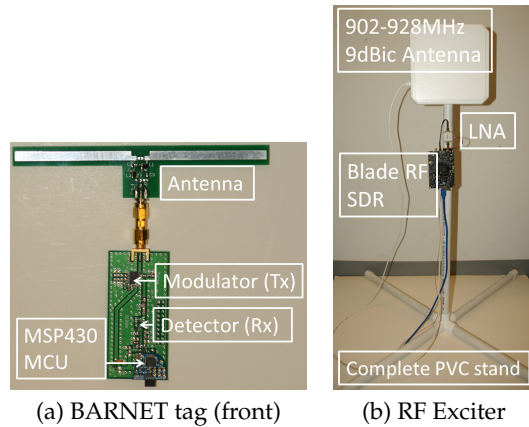


Figure 8: Prototypes BARNET tag and exciter used in the experiments

some of the tags will be operating at the minimum incident power, some of the tags will have higher incident power and the computation can be off-loaded to these tags. Additionally, power harvested at idle times and stored on super-capacitor can enable more complex computation at specific tags.

With power consumption about $3 \mu\text{W}$ and assumed 30% efficiency of power harvesting circuits [46], BARNET tags could operate from the harvested RF energy in the environment in which the input power is on the order of -20 dBm . The tag-to-tag link could operate at distance of 2 m if the Tx tag is also receiving at the least the same input power of -20 dBm [27]. Similar power levels have been considered in ambiently powered backscatter tag-to-tag networks [33, 39]. Lower power level is certainly possible, but will require careful power management beyond the scope of the current work.

5 PROTOTYPING AND EVALUATION

To demonstrate the feasibility of the backscatter channel characterization through the outlined BCSI measurement method and the utility of BCSI in recognizing human activities, we have implemented a prototype tag using discrete components on a PCB. This prototype tag enables a study and evaluation of the principle functions of the BARNET tags. The prototype tag includes a backscatter modulator for generation of the MPP signal and a passive radio-less demodulator that enables recording the received baseband signal for measurement of BCSI vector.

5.1 Prototype Tag Implementation

The implemented prototype tag with the basic functionality of the envisioned BARNET tag is shown in Figure 8(a). The prototype is a 2-layer FR4 printed circuit board (PCB) in thickness of 31 mils with components on both sides. A dipole antenna is implemented on a separate PCB that is attached to the main PCB using SMA connector. This modular design helps future experiments with different types of antennas.

In the PCB implementation, the multi-phase backscatter modulator consists of a 10-way RF switch (SP10T) SKY13404-466LF [6] driven by a low-power micro-controller MPS430 [7]. The switch poles are connected to 10 different load impedances to implement the 10 phase slots offering reflecting phases between $-\pi/2$ and $\pi/2$. Ideally, they should be uniformly spaced for better estimation of the BCSI features though it was not the case for the chosen impedances in the experiments for various practical constraints.

On the receiving end, to obtain a measure of the BCSI vector, we only have to extract the baseband signal. In Section 4, we proposed mixed-signal ASIC implementation that can measure the BCSI vector from the baseband signal with a very stringent power budget. For the PCB prototype, we obtain the same measure in the digital domain from a baseband signal digitized at high resolution. Although this approach can not be used in the passive ASIC implementation due to high power consumption and larger form factor, it provides a shorter implementation time and flexibility to study the proposed technique in the prototyping stage. To obtain the baseband signal, we first employ an envelope detection comprising a two stage voltage multiplier implemented using zero bias Schottky diode HSMS-285x series from Avago Technologies [4]. The output voltage signal of the envelope detector, the baseband signal, is converted to digital domain by a high-resolution 16-bit (full range 5 V) 80 kSamples/s analog-to-digital converter. The recorded signal is captured, transferred from tag to PC and stored in memory. From the digitized baseline signal, the BCSI vector is obtained by mimicking the architecture shown in Figure 7(b) in Matlab. Matlab implementation of the baseband signal processing to extract BCSI information enables exploring the tag and network design parameters on a real-world collected data. This will lead to optimization of the BARNET performance and design parameters of the BARNET tag implemented as ASIC. One example parameter is the resolution of on-chip ADCs, described in Section 4, where the resolution of the designed ADC is the trade-off between performance of the activity recognition algorithm, communication data rate and power budget.

The RF power is provided by an exciter as sufficient ambient RF power level is not available in our lab. The exciter only provides a fixed RF power and does not have any intelligence. For convenience, the exciter is implemented using a software radio platform (BladeRF [2]) and open source software [3] (Figure 8(b)). The BladeRF is connected to a host computer using USB3.0. In between BladeRF and Laird's 902-928MHz 9dBi circularly polarized antenna [1], we plug RF Bay's 915-LNA series [5] to amplify exciter signal to supply the required excitation power. The exciter operates at 915 MHz and the tag antenna and the matching circuit have been optimized to operate at this frequency.

5.2 BCSI vector measurement

Before analysis of the performance of the designed network for activity recognition with the prototype tags, we use the tags to evaluate the proposed BCSI measurement technique.

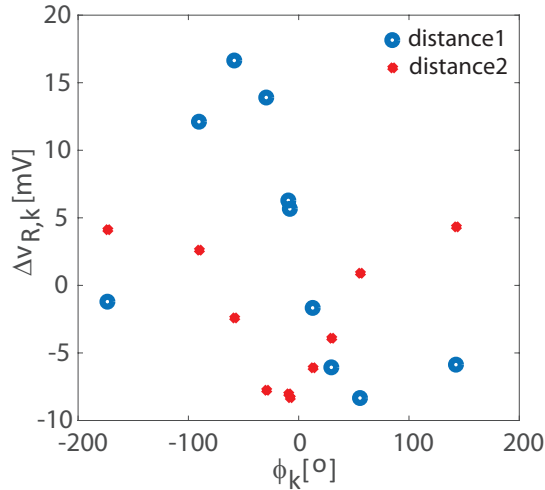
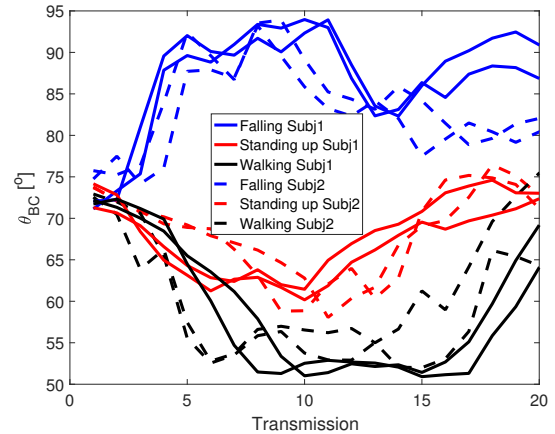


Figure 9: Amplitude difference $\Delta v_{R,k}$ as a function of modulation phase ϕ_k for two different distances between Tx-Rx tags

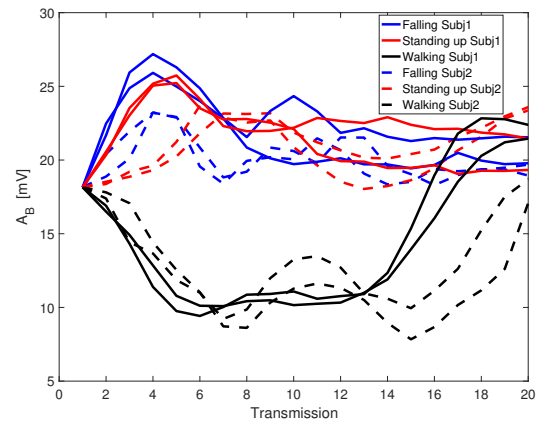
The implemented prototype tag enables collection of BCSI vector data for tag-to-tag link in a real-world scenario. We hypothesized in Section 3 that the BCSI information provides discriminatory features for recognition of activities in the vicinity of the tag-to-tag link. The classification task can then be performed using conventional machine learning algorithms.

We first verify that the amplitude difference, $\Delta v_{R,k}$, for a different modulation phase ϕ_k follows Eqn. (4). For this experiment, a Tx tag backscatters over ten phase slots and we monitor the voltage signal after the envelope detector in Rx tag by connecting the envelope detector output to a high-resolution ADC. The modulating phase spans the range from $-\pi$ to π . For two different distances between the tags, the amplitude difference $\Delta v_{R,k}$ is extracted and plotted as a function of the modulation phase ϕ_k in Figure 9. From the Figure, we can see that the amplitude difference follows Eqn. (3) and that for a different distance between the tags, amplitude and phase of backscatter channel can be easily extracted from measured $\Delta v_{R,k}$.

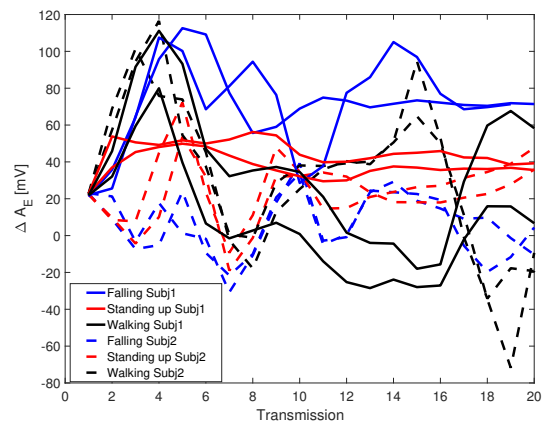
Next, we showcase the three components of BCSI vector that we extract and use for activity recognition in order to examine the patterns and repeatability in the feature vectors. The components of BCSI vector, as defined in Section 3.2, are the backscatter channel phase (θ_{BC}) and amplitude (A_B) and change in the excitation level ΔA_E . We have two subjects perform three different activities (falling, standing up and walking) in a lab setting, in a room of size 9 m × 9 m. The same protocol as in the previous experiment is used with Tx tag backscattering at 10 different phase slots. The baseband signal is recorded at Rx tag at 1.5 m distance from Tx tag. The sampling rate of the BCSI vector is 20 Hz and we observe for 1 s from the start of the activity. The time waveforms of the three components of BCSI vector are plotted in Figure 10 for two runs of the same activity by each subject. This set of plots illustrates how repeatable the feature vectors



(a) Backscatter channel phase



(b) Backscatter channel amplitude



(c) Change in excitation level

Figure 10: Components of the BCSI vector: Backscatter channel phase (θ_{BC}), amplitude (A_B) and change in the excitation level ΔA_E over time (i.e., successive transmissions of MPP packets)

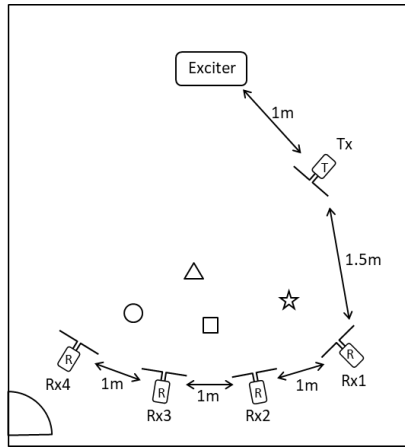


Figure 11: The experimental setup for the activity recognition study showing the locations of exciter and tags

are for a specific activity irrespective of the subject and how distinguishing patterns for different activities can be identified in the time waveforms. Note that it is possible that just one of the components of the BCSI vector is discriminating enough to distinguish specific activities. For example, in Figure 10(a), the channel phase time waveform is enough to discriminate between falling and standing up. But walking appears similar to standing up. On the other hand, walking and standing up are fairly distinguishable using amplitude (Figure 10(b)), while falling and standing up are similar. Similarly, while the changes in excitation level plot in Figure 10(c) appear noisy and provide little discriminatory power in the selected cases, it does provide distinguishing patterns in other cases which will be demonstrated in the following experiment. Overall, even visually, the three components of BCSI vector demonstrate considerable discriminatory power.

5.3 Activity Recognition

After verifying the proposed technique for the characterization of backscatter channel and visually inspecting the obtained BCSI feature vectors for distinguishing features, we conduct a study in which we evaluate the proposed technique for the activity recognition.

The study includes 9 participants (8 male, 1 female, ages 25–35, all healthy, physically fit and of average built) that perform 10 different daily activities. The activities are grouped into 8 classes: 1) brushing, 2) falling, 3) running, 4) no activity (person is either sitting or standing still), 5) sitting down from standing position, 6) standing up from seating position, 7) walking, 8) waving (person is either sitting or standing while waving). The activities are performed in a lab environment, in a room of size 9 m × 9 m. The room outline along with the positions of the RF exciter, Tx tag and four Rx tags and the selected positions of the subject performing the activity is shown in Figure 11.

The exciter power is set at 15 dBm. The Tx tag keeps transmitting MPP packets alternating between the 10 phase slots, as illustrated in Figure 6. Within each phase slot 16 Miller

encoded bits are transmitted at data rate of 10 kbps. The sampling time of the collection of BCSI information, that is the distance between subsequent MPP packets, is 50 ms and the data is recorded for 2.5 s from the start of the activity. The baseline signal is recorded at the sampling rate of 80 kSamples/s with 16 bit resolution at full 5 V range at each of Rx tags simultaneously. The recorded baseline signal is transferred to PC, where the off-line measurement of BCSI is performed prior to the classification. Each subject repeated 5 times each activity in each of 4 depicted locations in Figure 11. Overall 60+ minutes worth of activities are recorded for the training and classification.

While many forms of classifiers could be used, we chose the Convolutional Neural Networks (CNN) due to their wide use in the human activity recognition. Specifically, we use available tools for CNN for Human Activity Recognition (CNN for HAR) on the BCSI vector time series. We use available open source code multichannel CNN/HAR [53, 54]. We adopt the commonly used architecture of the CNN used for hand gesture recognition [14]. Since the input and output dimensions are simpler in BCSI based activity recognition, we have simplified the number of feature maps and sizes of convolution kernels. We have chosen the parameters in CNN $\kappa = 1, \alpha = 2 \times 10^{-4}, \beta = 0.75$ and followed the rules of thumb in [31] to choose other parameters.

One location in our experimental set up is selected as training location, and the other three locations are used for testing. We choose one of the subjects as the training subject and the others as testing. Figure 12(a) shows the average recognition accuracy for each of the activities with 1, 2, 3 or 4 receiving tags. Figure 12(b) shows the confusion matrix for the 4 tags case. Note that for the running and walking activities there are no separate training and testing locations as the activities are based on paths. The overall accuracy when all 4 tags are used is quite high, on average 94% across all cases. The accuracy is generally lower when a smaller number of tags are used. Clearly, more the number of tags more the accuracy (Section 3). Some activities such as falling, running and walking exhibit close to 100% accuracy even with just 1 tag. Some other activities (e.g., waving) have poor accuracy with 1 tag, but improves gradually with more tags. We expect further improvements with more tags. We expect significantly improved overall performance when many tag-to-tag links are used that we expect to be a common case in a typical BARNET deployment (Figure 1).

6 FEATURES AND LIMITATIONS

BARNET presents a vision of activity recognition based on the backscatter channel estimation of tag-to-tag links. We have demonstrated the feasibility of this approach by using prototype tags with the same functionality of the modulator/demodulator as the proposed BARNET tags. We also have demonstrated the location invariance, that is the location of the person performing the activity with respect to Tx and Rx tag has little or no effect on the feature vector and classification rate. We have not, however, fully quantified the

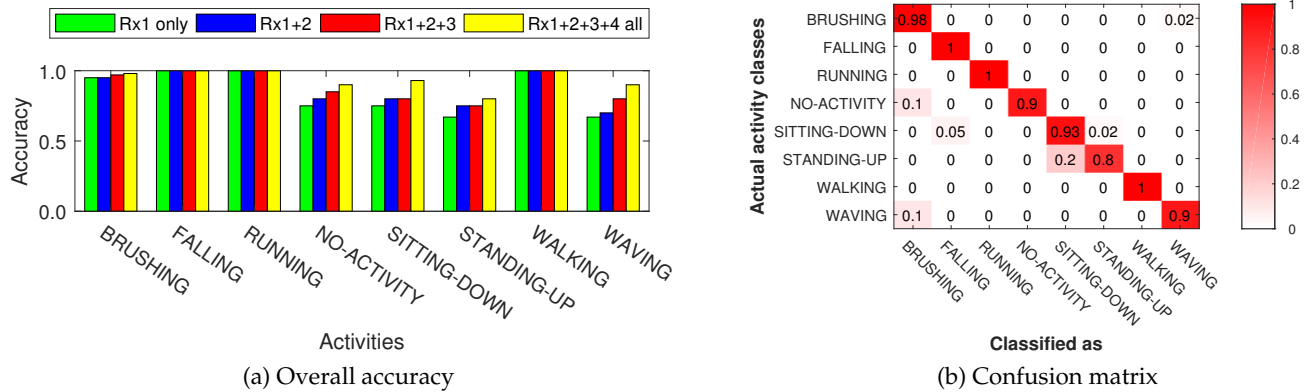


Figure 12: (a) Activity recognition accuracy for different activities with various sets of Rx tags (1, 2, 3 or 4 tags), (b) Confusion matrix for the 4 Rx tags case.

classification rate as a function of the location. Even so, due to the nature of feature BCSI vector that tracks the changes in the backscatter channel, the surrounding environment provides only an offset to all the three components in BCSI vector while the signature of a specific dynamic activity is preserved. This means that the network can be trained and tested in one environment and used in other environments without retraining. More extensive experiments are needed in order to provide quantification of the classification rate in both of these cases.

In the outlined experimental study, we have used a simple application scenario in which a preselected tag serves as Tx tag and the other present tags serve as Rx tags. As the number of the tags in the environment increases, the selection of the Tx and Rx tags becomes more elaborate as it is a function of latency in the network and available power budget at each of the tags. This topic is a subject of future work. If multiple tags are serving as Tx tags (the number of Rx tags does not affect the sampling rate), the transmission of MPP packets has to be time-multiplexed as all Tx-Rx channels have to obtain samples of the BCSI vector. The relatively slow moving human activities can be sampled at frequencies starting from 20 Hz as used in our current experiments. With the data rate of tag-to-tag link of 10 kbps and the number of phase slots on the order of 10, we can see that the number of Tx tag used in recognition of an activity can be rather large.

It is important to point out that a specific pair of Tx and Rx tags has a limited range in the surrounding of the tags in which the dynamic activity would cause substantial change in the backscatter channel with discriminative power. This means that the number of tags that would participate in a specific activity recognition is limited. This is especially important in a multi-person scenario. The performance of the system depends on the positioning of the users as well as the tags. If the network can find one or more tag-to-tag links that are influenced by one user and not by others, then there will be little influence on the performance. Given the inherent close range associated with backscattering tag-to-tag communication, this is likely to be the prevalent case in practice. However

if no link can be found that is influenced by the activity of only a single user, then the classification task could become challenging.

7 CONCLUSIONS

BARNET extends capabilities of passive RF tags to a different regime. They not only are able to perform tag-to-tag communications under conditions of very low modulation index, but also they are capable of channel measurements of the backscatter channel that correlates very well with environmental changes around the tags. This latter ability translates to human activity recognition. In our prototyping experiments BARNET tags' recognition accuracy is competitive with active radio-based techniques proposed in recent literature, while the tags use only passive techniques. The BARNET tags are designed to operate using harvested power from the externally provided RF signal and using only backscatter-based communication. We envision that BARNET-like RF tags will be essential components of future smart environments.

ACKNOWLEDGEMENT

This work is supported by US NSF grant CNS-1405740, by the MSIT, S.Korea, under the ICTCC Program (IITP-2017-R0346-16-1007) and S.Korea NRF grant (NRF-2017R1C1B 5075669). The authors are grateful to the anonymous reviewers and our shepherd (Jacob Sorber) for their valued comments and suggestions.

REFERENCES

- [1] 902-928 MHz 9 DBIC CIRCULAR POLARITY PANEL. <http://www.lairdtech.com/products/s9028pcl-s9028pcr>.
- [2] BladeRF: the USB 3.0 Superspeed Software Defined Radio. <http://nuand.com/>.
- [3] BladeRF USB 3.0 Superspeed Software Defined Radio Source Code. <https://nuand.com/forums/>.
- [4] HSMS-285x Series: Surface Mount Zero Bias Schottky Detector Diodes. <http://www.avagotech.com/docs/AV02-1377EN>.
- [5] LNA Series 902-928MHz Low Noise Amplifier. <http://rftbayinc.com/products.pdf/product.75.pdf>.
- [6] Skyworks SKY13404-466LF: 0.4-2.7 GHz SP10T Switch with GPIO Interface. <http://www.skyworksin.com/uploads/documents/201579E.pdf>.

- [7] Texas Instruments MSP430 family of ultra-low-power microcontrollers. <http://www.ti.com/lit/ds/slas491i/slas491i.pdf>.
- [8] ABDELNASSER, H., YOUSSEF, M., AND HARRAS, K. A. Wiggest: A ubiquitous wifi-based gesture recognition system. In *IEEE Conference on Computer Communications* (2015), INFOCOM '15, pp. 1472–1480.
- [9] ADIB, F., KABELAC, Z., AND KATABI, D. Multi-person localization via rf body reflections. In *12th USENIX Symposium on Networked Systems Design and Implementation* (2015), NSDI '15, pp. 279–292.
- [10] BHARADIA, D., JOSHI, K. R., KOTARU, M., AND KATTI, S. Backfi: High throughput wifi backscatter. In *Proceedings of the 2015 ACM Conference on Special Interest Group on Data Communication, SIGCOMM '15*, ACM, pp. 283–296.
- [11] BLETSAS, A., DIMITRIOU, A., AND SAHALOS, J. Improving backscatter radio tag efficiency. *IEEE Transactions on Microwave Theory and Techniques* 58, 6 (2010), 1502–1509.
- [12] BOYER, C., AND ROY, S. Space time coding for backscatter RFID. *IEEE Transactions on Wireless Communications* 12, 5 (2013), 2272–2280.
- [13] BOYER, C., AND ROY, S. Backscatter communication and RFID: Coding, energy, and mimo analysis. *IEEE Transactions on Communications* 62, 3 (2014), 770–785.
- [14] BULLING, A., BLANKE, U., AND SCHIELE, B. A tutorial on human activity recognition using body-worn inertial sensors. *ACM Computing Surveys* 46, 3 (2014), 33:1–33:33.
- [15] CHEN, G., GHAED, H., HAQUE, R.-U., WIECKOWSKI, M., KIM, Y., KIM, G., FICK, D., KIM, D., SEOK, M., WISE, K., ET AL. A cubic-millimeter energy-autonomous wireless intraocular pressure monitor. In *Solid-State Circuits Conference Digest of Technical Papers (ISSCC), 2011 IEEE International* (2011), IEEE, pp. 310–312.
- [16] CHEN, H.-Y., BHADKAMKAR, A., CHOU, T.-H., AND DER WEIDE, D. V. Vector backscattered signals improve piggyback modulation for sensing with passive uhf rfid tags. *IEEE Transactions on Microwave Theory and Techniques* 59, 12 (2011), 3538–3545.
- [17] DOBKIN, D. M. *The RF in RFID: Passive UHF RFID in Practice*. Newnes, 2007.
- [18] FINKENZELLER, K. *RFID Handbook: Fundamentals and Applications in Contactless Smart Cards and Identification*, 2nd ed. Wiley Publishing, 2003.
- [19] GAO, Q., WANG, J., MA, X., FENG, X., AND WANG, H. CSI-based device-free wireless localization and activity recognition using radio image features. *IEEE Transactions on Vehicular Technology* 66, 11 (2017), 10346–10356.
- [20] GRIFFIN, J., AND DURGIN, G. Complete link budgets for backscatter-radio and RFID systems. *IEEE Trans. on Antennas and Propagation Magazine* 51, 2 (2009), 11–25.
- [21] HALPERIN, D., HU, W., SHETH, A., AND WETHERALL, D. Predictable 802.11 packet delivery from wireless channel measurements. In *ACM SIGCOMM Computer Communication Review* (2010), vol. 40, ACM, pp. 159–170.
- [22] HAYKIN, S., MOHER, M., AND KOILPILLAI, D. *Modern Wireless Communications*. Pearson, 2011.
- [23] HONG, H.-C., AND LEE, G.-M. A 65-fj/conversion-step 0.9-v 200-ks/s rail-to-rail 8-bit successive approximation adc. *IEEE Journal of Solid-State Circuits* 42, 10 (2007), 2161–2168.
- [24] HUANG, X., AND DAI, M. Indoor device-free activity recognition based on radio signal. *IEEE Transactions on Vehicular Technology* 66, 6 (2017), 5316–5329.
- [25] HUITING, J., FLISIJN, H., KOKKELER, A. B. J., AND SMIT, G. J. M. Exploiting phase measurements of EPC Gen2 RFID tags. In *RFID-Technologies and Applications (RFID-TA), 2013 IEEE International Conference on* (2013), IEEE, pp. 1–6.
- [26] JEONG, S., CHEN, Y., JANG, T., TSAI, J. M.-L., BLAAUW, D., KIM, H.-S., AND SYLVESTER, D. Always-on 12-nw acoustic sensing and object recognition microsystem for unattended ground sensor nodes. *IEEE Journal of Solid-State Circuits* 53, 1 (2018), 261–274.
- [27] KARIMI, Y., ATHALYE, A., DAS, S., DJURIĆ, P., AND STANAČEVIĆ, M. Design of backscatter-based tag-to-tag system. In *IEEE International Conference on RFID* (2017), RFID '17.
- [28] KELLOGG, B., PARKS, A., GOLLAKOTA, S., SMITH, J. R., AND WETHERALL, D. Wi-fi backscatter: internet connectivity for RF-powered devices. In *Proceedings of the 2014 ACM Conference on Special Interest Group on Data Communication, SIGCOMM '14*, ACM, pp. 607–618.
- [29] KELLOGG, B., TALLA, V., AND GOLLAKOTA, S. Bringing gesture recognition to all devices. In *Proceedings of the 11th USENIX Conference on Networked Systems Design and Implementation* (2014), NSDI '14, pp. 303–316.
- [30] KIM, S. C. Device-free activity recognition using CSI big data analysis: A survey. In *2017 Ninth International Conference on Ubiquitous and Future Networks (ICUFN)* (2017), pp. 539–541.
- [31] LECUN, Y., BOTTOU, L., ORR, G. B., AND MÜLLER, K.-R. Efficient backprop. In *Neural Networks: Tricks of the Trade, This Book is an Outgrowth of a 1996 NIPS Workshop* (1998), Springer-Verlag, pp. 9–50.
- [32] LI, H., YE, C., AND SAMPLE, A. P. IDSense: A human object interaction detection system based on passive UHF RFID. In *Proceedings of the 33rd Annual ACM Conference on Human Factors in Computing Systems* (2015), CHI '15, pp. 2555–2564.
- [33] LIU, V., PARKS, A., TALLA, V., GOLLAKOTA, S., WETHERALL, D., AND SMITH, J. R. Ambient backscatter: Wireless communication out of thin air. In *Proceedings of the ACM Conference on Special Interest Group on Data Communication* (2013), SIGCOMM '13, pp. 39–50.
- [34] MA, K., LI, X., LIU, H., SHENG, X., WANG, Y., SWAMINATHAN, K., LIU, Y., XIE, Y., SAMPSON, J., AND NARAYANAN, V. Dynamic power and energy management for energy harvesting nonvolatile processor systems. *ACM Transactions on Embedded Computing Systems (TECS)* 16, 4 (2017), 107.
- [35] MARROCCO, G., AND CAZZONE, S. Electromagnetic models for passive tag-to-tag communications. *IEEE Transactions on Antennas and Propagation* 60, 11 (2012), 5381–5389.
- [36] NADERIPARIZI, S., PARKS, A. N., KAPETANOVIC, Z., RANSFORD, B., AND SMITH, J. R. Wispcam: A battery-free rfid camera. In *RFID (RFID), 2015 IEEE International Conference on* (2015), IEEE, pp. 166–173.
- [37] NIKITIN, P., RAMAMURTHY, S., MARTINEZ, R., AND RAO, K. Passive tag-to-tag communication. In *IEEE International Conference on RFID* (2012), RFID '12, pp. 177–184.
- [38] PARADA, R., MELIÀ-SEGÚ, J., CARRERAS, A., MORENZA-CINOS, M., AND PONS, R. Measuring user-object interactions in IoT spaces. In *IEEE International Conference on RFID Technology and Applications* (2015), RFID-TA '15, pp. 52–58.
- [39] PARKS, A. N., LIU, A., GOLLAKOTA, S., AND SMITH, J. R. Turbocharging ambient backscatter communication. In *Proceedings of the 2015 ACM Conference on Special Interest Group on Data Communication* (2014), SIGCOMM '14, pp. 619–630.
- [40] PINUELA, M., MITCHESON, P. D., AND LUCYSZYN, S. Ambient rf energy harvesting in urban and semi-urban environments. *IEEE Transactions on Microwave Theory and Techniques* 61, 7 (2013), 2715–2726.
- [41] PU, Q., GUPTA, S., GOLLAKOTA, S., AND PATEL, S. Whole-home gesture recognition using wireless signals. In *Proceedings of the 19th Annual International Conference on Mobile Computing Networking* (2013), MobiCom '13, pp. 27–38.
- [42] RYOO, J., JIAN, J., ATHALYE, A., DAS, S., AND STANAČEVIĆ, M. Design and evaluation of BTTN – a backscattering tag-to-tag network. *IEEE Internet of Things Journal*. Accepted for publication, to appear.
- [43] SAUERBREY, J., SCHMITT-LANDSIEDEL, D., AND THEWES, R. A 0.5-v 1-/spl mu/w successive approximation adc. *IEEE Journal of Solid-State Circuits* 38, 7 (2003), 1261–1265.
- [44] SHEN, Z., ATHALYE, A., AND DJURI, P. M. Phase cancellation in backscatter-based tag-to-tag communication systems. *IEEE Internet of Things Journal* 3, 6 (2016), 959–970.
- [45] SIGG, S., BLANKE, U., AND TROSTER, G. The telepathic phone: Frictionless activity recognition from wifi-rssi. In *IEEE International Conference on Pervasive Computing and Communications* (2014), PerCom '14, pp. 148–155.
- [46] STOOPMAN, M., KEYROUZ, S., VISSER, H. J., PHILIPS, K., AND SERDIJN, W. A. Co-design of a cmos rectifier and small loop antenna for highly sensitive RF energy harvesters. *IEEE Journal of Solid-State Circuits* 49, 3 (2014), 622–634.
- [47] THOMAS, S., WHEELER, E., TEIZER, J., AND REYNOLDS, M. Quadrature amplitude modulated backscatter in passive and semipassive UHF RFID systems. *IEEE Transactions on Microwave Theory and Techniques* 60, 4 (2012), 1175–1182.
- [48] VITA, G. D., AND IANNACCONE, G. Design criteria for the rf section of uhf and microwave passive rfid transponders. *IEEE Transactions on Microwave Theory and Techniques* 53, 9 (2005), 2978–2990.
- [49] WANG, J., ZHANG, X., GAO, Q., YUE, H., AND WANG, H. Device-free wireless localization and activity recognition: A deep learning approach. *IEEE Transactions on Vehicular Technology* 66, 7 (July 2017), 6258–6267.
- [50] WANG, W., LIU, A. X., SHAHZAD, M., LING, K., AND LU, S. Understanding and modeling of wifi signal based human activity recognition. In *Proceedings of the 21st Annual International Conference on Mobile Computing and Networking* (2015), MobiCom '15, pp. 65–76.
- [51] WANG, Y., LIU, J., CHEN, Y., GRUTESER, M., YANG, J., AND LIU, H. E-eyes: Device-free location-oriented activity identification using fine-grained wifi signatures. In *Proceedings of the 20th Annual International Conference on Mobile Computing and Networking* (2014), MobiCom '14, pp. 617–628.
- [52] XIAO, Y. IEEE 802.11n: enhancements for higher throughput in wireless LANs. *IEEE Wireless Communications* 12, 6 (2005), 82–91.
- [53] YANG, J. CNN-timeseries: Use CNN to classify time series data for activity recognition. <https://github.com/sibosutd/cnn-timeseries>, 2017.

- [54] YANG, J. B., NGUYEN, M. N., SAN, P. P., LI, X. L., AND KRISHNASWAMY, S. Deep convolutional neural networks on multichannel time series for human activity recognition. In *Proceedings of the 24th International Conference on Artificial Intelligence (2015), IJCAI '15*, pp. 3995–4001.
- [55] YOUSEFI, S., NARUI, H., DAYAL, S., ERMON, S., AND VALAEE, S. A survey of human activity recognition using wifi CSI. *CoRR abs/1708.07129* (2017).